IEEE Access
Multidisciplinary | Rapid Review | Open Access Journal

Received 28 May 2023, accepted 7 June 2023, date of publication 16 June 2023, date of current version 21 June 2023.

Digital Object Identifier 10.1109/ACCESS.2023.3286868

RESEARCH ARTICLE

Realization of Control Algorithm for Vehicle Optoelectronic Tracking Platform Based on Sliding Mode Control and Active Disturbance Rejection Control Optimized by Differential Evolution Algorithm

ZHAOLONG WU[1,2], ZHAOBING CHEN[1], BOHAN XU[1], SHUSHUAI PANG[1], AND FENG LIN[1]

[1]Changchun Institute of Optics, Fine Mechanics and Physics, Chinese Academy of Sciences, Changchun 130033, China
[2]University of Chinese Academy of Sciences, Beijing 100049, China

Corresponding author: Zhaobing Chen (chenzhaobing@ciomp.ac.cn)

ABSTRACT In order to improve the tracking ability of the vehicle mounted photoelectric tracking platform, and make its tracking system has the characteristics of rapid response, small overshoot, high-precision position tracking, strong anti-interference and good robustness. In this paper, a joint active disturbance rejection control (ADRC) and sliding mode control (SMC) method is proposed, which can effectively improve the tracking ability of the equipment. Firstly, the mathematical model of the DC motor is analyzed, and then the sliding mode control based on the linear extended state observer (LESO) and the third-order tracking differentiator is established as the speed loop control of the system. Finally, the parameters of the nonlinear ADRC which built control system's position loop are optimized by the improved differential evolution (DE) algorithm. The speed loop simulation results show that the proposed algorithm has better control effect than PID control algorithm, Robust control algorithm, and ADRC control algorithm;The simulation of position loop demonstrates that the performance of the controller optimized by DE algorithm is better than the parameter tuning based on experience. The experimental results illustrate that the proposed control algorithm can ensure that the optoelectronic tracking equipment can track the target which 3km away with 0.1 mrad accuracy.

INDEX TERMS ADRC, SMC, differential evolution, DC-motor, opto-electronic tracking and pointing servo control.

I. INTRODUCTION

The Optoelectronic tracking platform is widely used in military, astronomical observation, laser communication and other fields [1], [2], [3]. The task requires that the position accuracy of the equipment is getting higher and higher, and the equipment also needs to have fast response capability when facing high-speed and highly mobile targets. When undertaking the tracking task on the moving platform, the equipment will inevitably be affected by external disturbances, so the servo control algorithm needs to have the anti-interference ability. These increasingly demanding index requirements and complex and changeable use environments bring great challenges to the design of control algorithms.

Han's ADRC [4] consists of the tracking differentiator (TD), the extended state observer (ESO) and the nonlinear state error feedback law (NLSEF). TD not only arranges the transition process, but also reduces the impact of noise on the numerical derivation. ESO is a new idea for compensating system disturbances. Then, Gao [5] successfully associated the linearly extended state observer (LESO) with the frequency domain, using the concept of observer bandwidth to

The associate editor coordinating the review of this manuscript and approving it for publication was Tianhua Xu.

reduce the number of observer parameters and increase the engineering practicality. Nonlinear extended state observers can be more efficient than LESO in estimating the system, but their parameters are difficult to tune. Therefore, there are neural network-based methods [6], [7], [8] to tune the system parameters online, making the system adaptive and improving the robustness of the system, but this also puts high demands on the hardware computing power. In addition, there are a large number of examples of optimization-based algorithms for parameter tuning, such as genetic algorithm (GA) [9], [10], [11], differential evolutionary (DE) algorithm [12], [13], [14] and particle swarm algorithm [15]. The system performance is significantly improved with these methods.

A well-parameterized extended state observer can estimate the system state with high accuracy, which provides effective information for the controller. In [16], a velocity loop controller for permanent magnet synchronous motor (PMSM) is designed using ESO joint sliding mode control (SMC), and its results indicate that the robustness and control efficiency of the system are greatly enhanced. Reference [17] also demonstrated that ESO-based sliding mode control is more efficient than ADRC and sliding mode control.while not increasing the complexity of the control law. Reference [18] improved the ESO-based SMC using Smith predictor. Comparing the ADRC controller, improved controller response is faster and the system robustness and stability is better. Reference [19] Added known information to ESO for observing disturbances. The SMC controller performs a promising behavior using the observed information. These studies all illustrate that using SMC instead of the NLSEF in ADRC can improve the general behavior of the control system.

Thus, this paper proposes a SMC law based on ESO and TD and an ADRC control algorithm using an improved differential evolutionary algorithm to optimize the parameters of controller. This paper is organized as follows. Section II is the establishment of the mathematical model of the controlled object. Section III is the design of the control algorithm for the optoelectronic tracking equipment, in which the velocity loop uses a sliding mode control combining ESO and third-order TD, and the position loop is an ADRC controller with parameter tuning based on an improved differential evolutionary algorithm. Section IV is a computer simulation based on Matlab/simulink. Section V is to conduct experiments to verify the effectiveness of the control algorithm. The final summary is in section VI.

II. ANALYSIS OF THE MATHEMATICAL MODEL OF THE CONTROLLED OBJECT

The establishment and analysis of the controlled object model is the most important step in designing a control system. DC torque motor has the advantages of large torque, low speed, good linearity, no need to equip with reducer, etc., and considering the demand of miniaturization of optoelectronic equipment, so DC torque motor is used as the actuator of optoelectronic platform. The equation of motion of a DC torque motor can be described as:

$$\begin{aligned} U_a(t) &= R_a I_a(t) + L_a \frac{dI_a(t)}{dt} + K_b\omega \\ J_m \frac{d\omega}{dt} &= K_m I_a(t) - T \end{aligned} \tag{1}$$

where $U_a(t)$, $I_a(t)$, R_a and L_a are voltage, current, resistance and inductance of armature, respectively; K_b and K_m denote back EMF coefficient and torque coefficient. ω and J_m represent DC motor rotor's angle speed and moment of inertia of the rotor and frames. T represents external torque disturbance.

According to (1), the transfer function of the DC motor can be obtained:

$$\begin{aligned} G(s) &= \frac{\omega(s)}{u_a(s)} = \frac{1/K_b}{T_e T_m s^2 + T_m s + 1} \\ T_e &= \frac{L_a}{R_a}, \quad T_m = \frac{J_m R_a}{K_b K_m} \end{aligned} \tag{2}$$

where T_e, T_m represent Electrical time constant and Mechanical time constant. Let system's states $X = [\omega, \dot{\omega}]'$, input $u = u_a$,$d(t)$ is perturbations such as system model ingestion, external disturbances and combined external torques. Then the DC motor state space equation from (2) can be described as:

$$\begin{aligned} &\dot{X} = A \cdot X + B \cdot u + D \\ &Y = C \cdot X \\ &A = \begin{bmatrix} 0, & 1 \\ -\frac{1}{T_e \cdot T_m}, & -\frac{1}{T_e} \end{bmatrix} B = \begin{bmatrix} 0 \\ \frac{1}{K_b * T_m * T_e} \end{bmatrix} \\ &C = \begin{bmatrix} 1 \ , \ 0 \end{bmatrix} \\ &D = [0, d(t)]' \quad ||d(t)||_2 < \infty \end{aligned} \tag{3}$$

III. CONTROLLER DESIGN FOR TRACKING SYSTEMS

A. SPEED LOOP

Design the sliding mode control law according to the controlled object (3), and the sliding surface is selected as:

$$\begin{aligned} s &= c \cdot e + \dot{e}, c > 0 \\ e &= \omega - \omega_r \end{aligned} \tag{4}$$

where ω, ω_r are the rotor's angle speed and desired speed. To satisfy the sliding mode existence and approachability conditions, the time derivative of the sliding variable is [20]:

$$\dot{s} = -\eta \cdot sgn(s) - k \cdot s \quad (\eta > 0, k > 0) \tag{5}$$

According to sliding mode control theory [21], decreasing η and increasing k can accelerate the convergence process. Let the Lyapunov function of the system is:

$$\begin{aligned} V(t) &= \frac{1}{2} \cdot s^2 \\ \dot{V}(t) &= s \cdot \dot{s} \\ &= s \cdot (c \cdot \dot{e} + \ddot{e}) \\ &= s \cdot (c \cdot \dot{e} - \frac{1}{T_e \cdot \ T_m} \cdot \omega - \frac{1}{T_e} \cdot \dot{\omega} \end{aligned} \tag{6}$$

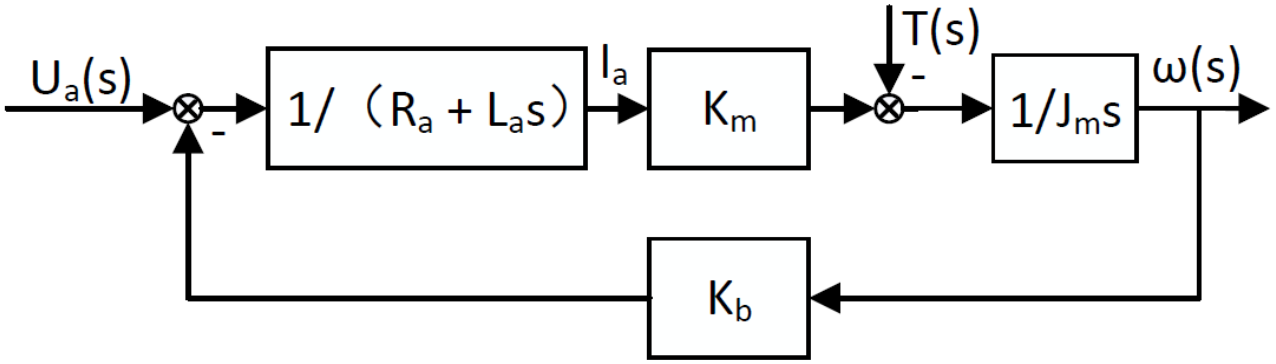

FIGURE 1. Block diagram of DC motor system.

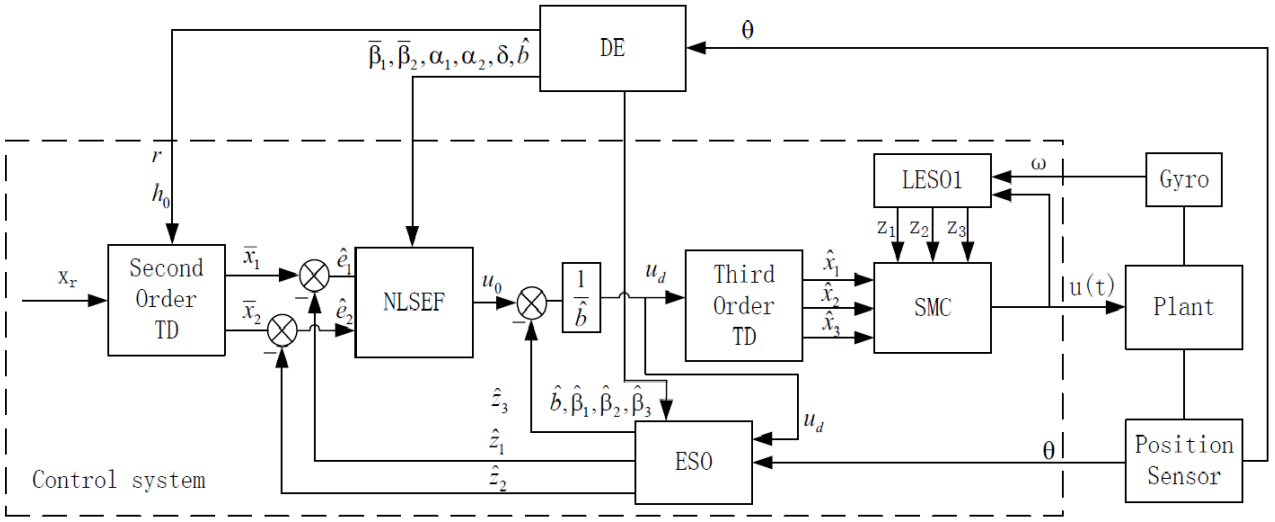

FIGURE 2. Double closed-loop control system.

$$+\frac{1}{K_b \cdot T_m \cdot T_e} \cdot u(t) - \ddot{\omega}_r + d(t)) \tag{7}$$

Then, from equations (7) and (5), we can deduce that the system input is:

$$u(t) = K_b T_m T_e \cdot [-c \cdot \dot{e} + \frac{1}{T_e \cdot T_m} \cdot \omega + \frac{1}{T_e} \cdot \dot{\omega} + \ddot{w}_d - d(t) - \eta \cdot sgn(s) - k \cdot s] \tag{8}$$

And (7) becomes:

$$\begin{aligned} \dot{V} &= s \cdot \dot{s} \\ &= s \cdot (-\eta \cdot sgn(s) - k \cdot s) \\ &= -\eta \cdot |s| - k \cdot s^2 \leq 0 \quad \forall \eta > 0 and \forall k > 0 \end{aligned} \tag{9}$$

From (9), it can be seen that the system is stable when the input takes(8). However, the input $u(t)$ contains an unknown perturbation term $d(t)$ and the derivative term of the feedback signal, which poses a greater difficulty in implementing the control law. This requires, first, that the external disturbance of the system needs to be estimated in real time, and second, that the derivative of the feedback signal is accurately calculated.

From the ADRC theory [22], it is known that the LESO is:

$$\begin{cases} e = z_1 - y \\ \dot{z}_1 = z_2 - 3\omega_0 e \\ \dot{z}_2 = z_3 - 3\omega_0^2 e + bu \\ \dot{z}_3 = -\omega_0^3 e \end{cases} \tag{10}$$

where z_1, z_2 are the observed values of the state variables in (3), respectively. z_3 represents the general perturbation in the ideal series integration system (11):

$$\begin{cases} \dot{x}_1 = x_2 \\ \dot{x}_2 = x_3 + bu \\ x_3 = f(x_1, x_2, t) \end{cases} \tag{11}$$

$$z_3 = -\frac{1}{T_e \cdot T_m} \cdot x_1 - \frac{1}{T_e} \cdot x_2 + d(t) \tag{12}$$

ω_0 is denoted as the bandwidth of the LESO.$b = 1/(K_b \cdot T_m \cdot T_e)$. When the state of the system is observed by LESO, the

system speed loop input becomes:

$$u(t) = \frac{1}{b} \cdot [-c \cdot \dot{e} + \ddot{w}_d - z_3 - \eta \cdot sgn(s) - k \cdot s] \quad (13)$$

For the control law shown in (13), a third-order TD is also required to implement the derivative calculation of its input signal. The third-order TD is given by [23]:

$$\begin{cases} \dot{\hat{x}}_1 = \hat{x}_2 \\ \dot{\hat{x}}_2 = \hat{x}_3 \\ \dot{\hat{x}}_3 = -R \cdot sat(\hat{x}_1 - u_d - \frac{\hat{x}_3^2}{6R^2} + A(\frac{\hat{x}_3}{R} + S\sqrt{\frac{A}{R}}), \delta) \\ S = sign(\hat{x}_2 + \frac{|\hat{x}_3|\hat{x}_3}{2R}) \\ A = S \cdot \hat{x}_2 + \frac{\hat{x}_3^2}{2R} \end{cases} \quad (14)$$

where R and δ are parameters to be regulated. u_d is the input to be tracked. $\hat{x}_1, \hat{x}_2, \hat{x}_3$ are the trace value of the input instruction, the derivative of the input instruction and the second-order derivative of the input instruction, respectively. So the control law of the speed loop becomes:

$$\begin{aligned} u(t) &= \frac{1}{b} \cdot [-c \cdot (z_2 - \hat{x}_2) + \hat{x}_3 - z_3 - \eta \cdot sign(\hat{s}) - k \cdot \hat{s}] \\ \hat{s} &= c \cdot (z_1 - \hat{x}_1) + z_2 - \hat{x}_2 \end{aligned} \quad (15)$$

B. POSITION LOOP

1) ADRC

ADRC is the compensation of the system into a series-integral type by ESO and NLSEF. The second-order discrete TD can be expressed as:

$$\begin{cases} \bar{x}_1(k+1) = \bar{x}_1(k) + h \cdot \bar{x}_2(k) \\ \bar{x}_2(k+1) = \bar{x}_2(k) + h \cdot fh \\ fh = fhan(\bar{x}_1(k) - v_0, \bar{x}_2(k), r, h_0) \end{cases} \quad (16)$$

$$\begin{cases} fhan = -\begin{cases} r \cdot sign(\alpha_0) & |\alpha_0| > rh_0 \\ \alpha_0/h & |\alpha_0| \le rh_0 \end{cases} \\ \alpha_0 = \begin{cases} \bar{x}_2 + \frac{1}{2}(\sqrt{8r|y| + r^2h_0^2} - \\ rh_0) \cdot sign(y) & |y| > rh_0^2 \\ \bar{x}_2 + \frac{y}{h_0} & |y| \le rh_0^2 \end{cases} \\ y = \bar{x}_1 - v_0 + h_0\bar{x}_2 \end{cases} \quad (17)$$

The third-order ESO can be shown as:

$$\begin{cases} e_1(k) = \hat{z}_1(k) - y(k) \\ \hat{z}_1(k+1) = \hat{z}_1(k) + h \cdot (-\hat{\beta}_1 e_1(k) + \hat{z}_2(k)) \\ \hat{z}_2(k+1) = \hat{z}_2(k) + h \cdot (-\hat{\beta}_2 fal(e_1(k), 0.5, h) \\ \qquad + \hat{b}u(k) + \hat{z}_3(k)) \\ \hat{z}_3(k+1) = \hat{z}_3 - h\hat{\beta}_3 fal(e_1(k), 0.25, h) \end{cases} \quad (18)$$

$$fal(e_1, \alpha, \delta) = \begin{cases} \frac{e_1}{\delta^{1-\alpha}} & |e_1| \le \delta \\ |e_1|^\alpha sign(e_1) & |e_1| > \delta \end{cases} \quad (19)$$

The NLSEF can be given as:

$$\begin{cases} \hat{e}_1 = \bar{x}_1 - \hat{z}_1 \\ \hat{e}_2 = \bar{x}_2 - \hat{z}_2 \\ u_0 = \bar{\beta}_1 fal(\hat{e}_1, \alpha_1, \delta) + \bar{\beta}_2 fal(\hat{e}_2, \alpha_2, \delta) \\ u_d(k) = \frac{u_0 - \bar{z}_3}{b} \end{cases} \quad (20)$$

When compensated by the speed loop and output limiting, the model of the system has become complex. However, the system can be approximated as a second-order system with respect to x_1, x_2. The controlled object is:

$$\begin{cases} \dot{x}_1 = x_2 \\ \dot{x}_2 = f(x_1, x_2, t) + \hat{b}u_d \end{cases} \quad (21)$$

Therefore, the position loop of the controlled system can be designed as second-order ADRC, and the structure of its control system is shown in Fig.2. For nonlinear ADRC, although the control capability of the system is improved, the parameter tuning also becomes very troublesome. To simplify the process of parameter tuning and to obtain the approximate distribution ranges of parameters for the reference of actual parameter tuning, the differential evolution algorithm is used for the tuning of system parameters.

2) DIFFERENTIAL EVOLUTION ALGORITHM

The differential evolutionary algorithm is inspired by the survival of the fittest in nature, where individuals in a population are mutated, crossed and selected to simulate population evolution, and evolve generation by generation until a global optimal solution is found.

$$\boldsymbol{X_{i,G}} = (x_{1,i,G}, x_{2,i,G}, \ldots, x_{L,i,G}) \quad (22)$$

The formula (22) represents the i-th individual in the Gth generation of the population, meaning a solution in the solution space, while L represents the dimensionality of the problem, which means the number of independent solution variables.

The population initialization can be described as:

$$x_{j,i,0} = x_{j,i}^{min} + rand(0, 1) \times (x_{j,i}^{max} - x_{j,i}^{min}) \quad (23)$$

In formula (23), $x_{j,i}^{max}$ and $x_{j,i}^{min}$ mean the optimization zone for the j-th optimization parameter. Once the initial population is established, the population can begin to evolve iteratively. The most critical part of this process is the mutation and crossover.

$$\boldsymbol{V_{i,G}} = \boldsymbol{X_{r1,G}} + F \cdot (\boldsymbol{X_{r2,G}} - \boldsymbol{X_{r3,G}}) \quad (24)$$

Equation (24) represents the mutation process, where $X_{r_1,G}, X_{r_2,G}, X_{r_3,G}$ are the random individuals in the population, and F is the scaling factor.

$$u_{j,i,G} = \begin{cases} V_{j,i,G}, & \text{rand(0,1)} \le \text{CR} \\ X_{j,i,G}, & \text{otherother} \end{cases} \quad (25)$$

where CR denotes the crossover factor. The next generation is selected based on the fitness function, and those with high fitness are inherited to the next generation.

$$\boldsymbol{X_{i,GC1}} = \begin{cases} \boldsymbol{U_{i,G}}, & \text{f}(X_{i,G}) \le \text{f}(U_{i,G}) \\ \boldsymbol{X_{i,G}}, & \text{other} \end{cases} \quad (26)$$

The fitness function is taken to be:

$$f = \sum \omega_i J_i \quad (\sum \omega_i = 1) \quad (27)$$

$$J_1 = \int t|e|dt \tag{28}$$

$$J_2 = 2 * \frac{1}{1 + \text{rise time/total time}} - 1 \tag{29}$$

$$J_3 = \frac{1}{1 + 100 \cdot \text{overshoot}} \tag{30}$$

$$J_4 = 2 * \frac{1}{1 + \text{settling time/total time}} - 1 \tag{31}$$

Equation (28) is criterion of the integral of time and absolute error (ITAE). Equation (29) is to measure the rapid response capability of the system. The formula (30) is to ensure that the overshoot of the system is as small as possible with the rapid response. The equation (31) is to guarantee that the settling time during the system response is as long as possible. total time indicates the total running time. The linear accumulation of them together constitutes the fitness function of the differential evolutionary algorithm. By adjusting the weights ω_i in (27), the focus on different indicators can be achieved.

When the differential evolution algorithm is designed, the faster the population changes when the crossover factor CR is selected, but the damage to the best adapted individuals is also greater. Conversely, the population evolves slowly and the search speed of the solution decreases. Thus, the cross factor CR reflects the global search ability and local search ability of the algorithm. The scaling factor F is related to the convergence speed of the algorithm. Referring to [24], change CR and F to be about generational adaptive change.

$$CR = \frac{CR_{min}}{1 + (CR_{min}/CR_{max} - 1) \times exp(-k_1 \cdot G)} \tag{32}$$

$$F = \frac{F_{min}}{1 + (F_{min}/F_{max} - 1) \times exp(-k_2 \cdot G)} \tag{33}$$

Considering that there may be a relatively large range of controller parameters to choose from, roughly five orders of magnitude. Thus, for the optimized parameters the transformation is as follows:

$$\boldsymbol{x_{opt}} = 10^{X_{i,G}} \tag{34}$$

where x_{opt} is the parameter to be optimized in the controller. Such a transformation allows the solution to be distributed as widely as possible throughout the solution space for a finite population size. At the same time, a small change in $X_{i,G}$ causes a large variation in x_{opt}, which can increase the solution accuracy.

IV. SIMULATION AND ANALYSIS

A. SIMULATION OF SPEED LOOP

In order to verify the proposed method, this simulation is run on matlabR2020b/SIMULINK.The motor parameters are shown in Table 1. Controller parameters are shown in Table 2. Assume that the unknown perturbation $d(t) = sin(4 \cdot \pi t)$. ADRC feedback control law uses linear PD form, where $u(t) = ((\hat{\beta}_{s1} \cdot e_1 + \hat{\beta}_{s2} \cdot e_2) - z_3)/b$. The design methodology for PID controller is based on [25]. Robust controller is designed with reference to [26]. The noise in the speed feedback value is given according to the actual gyro situation, and the output is limited considering the actual situation. Tracking the given signal separately:1.Tracing $sin(20\pi t)$ and $sin(120\pi t)$ at $d(t) = 0$. Tracking a unit step signal at $d(t) = 0.5 \cdot 1(t - 0.5)$ where 1(t) is unit step. 3. Tracking the unit step signal and $sin(20\pi t)$ at $d(t) = sin(4\pi t)$. To compare the differences in performance of the simulation algorithms more accurately, the integral absolute value of the tracking error (IAE, $\int |e|dt$), the overshoot, the settling time (error less than 4% of the given value), and the rise time (the difference between the time to first reach 10% of the given value and the time to first reach 90% of the given value) are used to quantify the analysis.

As shown in Fig.3, Fig. 4, and Table 3, the robust control algorithm performs best when tracking sinusoidal signals. Both the ADRC controller and the SMC controller amplify the amplitude when tracking low frequency signals. Whereas all of the above algorithms show a noticeable decrease in

TABLE 1. Parameters of DC motor.

Item	Value	Unit
R_a	0.36	Ω
L_a	1.33e-3	H
K_b	0.099	V/(rad/s)
K_m	0.0989	$N \cdot m/A$
J	0.04016	$Kg \cdot m^2$

TABLE 2. Parameters of controller.

Item	Value
c	500
K	500
$\hat{\beta}_{s1}$	1000000
$\hat{\beta}_{s2}$	10000
λ	0.0025
η	1
A	0.1
K_1	50
K_2	30

TABLE 3. IAE values for different controllers.

Signal	SMC	PID	ADRC	ROBUST
sin(20π t) with d(t)=0	0.01077	0.09953	0.01353	0.00220
sin(120π t) with d(t)=0	0.20701	0.45087	1.05478	0.01683
Step with d(t)=0	0.003896	0.005582	0.00529	0.00643
Step with d(t)= 0.5*1(t-0.5)	0.00480	0.00858	0.00560	0.00854
Step with d(t)=sin(4π t)	0.00380	0.005537	0.00529	0.00643
sin(20π t) with d(t)= sin(4π t)	0.01076	0.09953	0.01352	0.00219

TABLE 4. Time domain indicators of the step response.

Item		SMC	PID	ADRC	ROBUST
Step with d(t)=0	overshoot(%)	4.3	13.2	2.2	70.9
	settling time(s)	0.0116	0.0345	0.0079	0.0277
	rise time(s)	0.0020	0.0021	0.0035	0.00087
Step with d(t)=sin(4πt)	overshoot(%)	4.3	13.0	2.3	71.2
	settling time(s)	0.0116	0.0345	0.0079	0.0277
	rise time(s)	0.002	0.0022	0.0036	0.00088

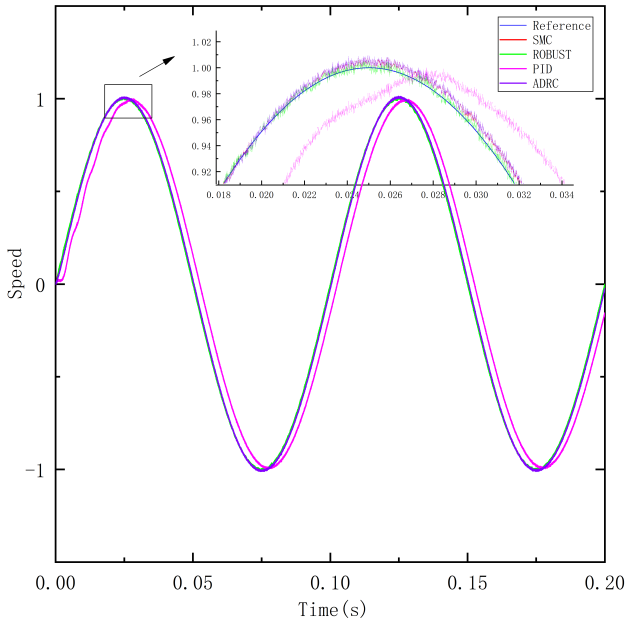

FIGURE 3. The response results of the tracking $sin20\pi t$.

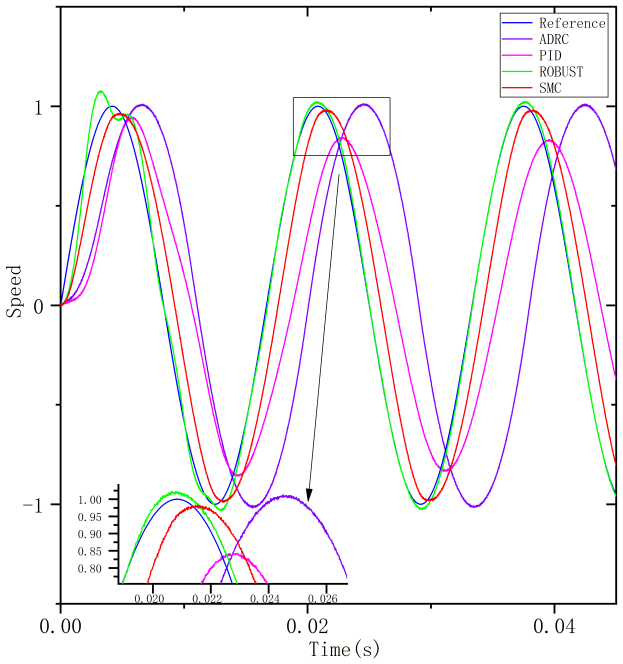

FIGURE 4. The response results of the tracking $sin120\pi t$.

tracking accuracy when tracking high frequency sinusoidal signals, where the PID and ADRC controllers have significantly less bandwidth than the SMC and robust controllers. The enhancement of the speed loop bandwidth by the SMC and robust controller will greatly improve the tracking capability of the phototracking system. It is worth noting that in this, the SMC controller is less accurate than the robust controller, due to the phase and accuracy losses in the estimates calculated by TD and ESO compared to the true values.

The controller parameters are held constant and the unit step signal is tracked without applying a disturbance. The

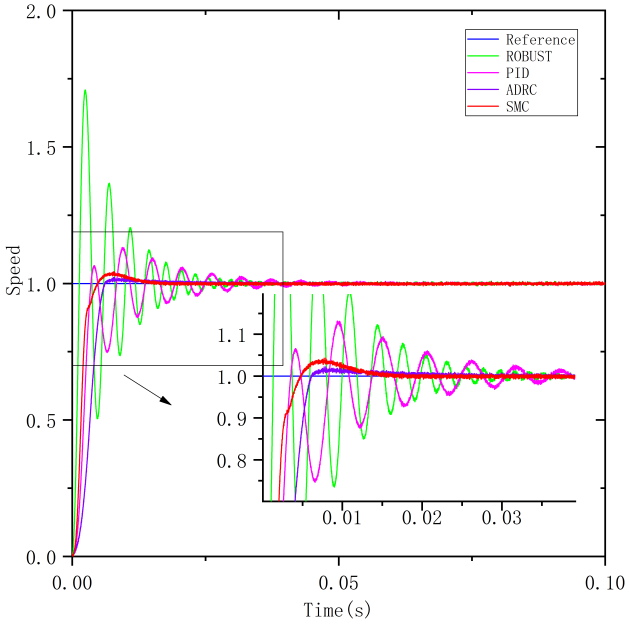

FIGURE 5. The response results of the tracking unit step.

tracking results are shown in Table3, Table4, and Fig.5. In terms of rise time, the robust controller responds the fastest, but it also causes the greatest overshoot, and it is found in the tuning that no matter how the parameters are tuned there is a large overshoot and oscillation in the case of guaranteed stable accuracy. The excessive overshoot of the robust controller does not facilitate the tracking of the target by the optoelectronic system. The PID controller and SMC response times are similar, but the response results for the PID controller show a conflict between rapidity and overshoot. The ADRC algorithm has a short response time to enter the steady state quickly, but its accuracy is comparable to that of the PID, indicating that its error after stabilisation does not converge to a small value.

The results shown in Fig.7, Fig.6, and Fig.8 illustrate the ability of the controller against external disturbances. ADRC and SMC show similar anti-perturbative effects in the face of step disturbances, while both robust controller and PID controller show large oscillations when suppressing disturbances, which is not conducive to system stability. Comparing before and after the application of the periodic perturbation, it can be seen that the perturbation has no significant effect on the tracking accuracy. This illustrates that the control algorithms are all able to suppress the disturbances well in the face of low frequency periodic disturbances. The above simulation comparison demonstrates that the SMC controller proposed in this paper can absorb the advantages of the ADRC controller and improve the tracking capability of the system dramatically.

B. SIMULATION OF POSITION LOOP AND DE ALGORITHM

The control system is built up in Matlab/Simulink and white noise is added to the model according to the noise intensity of the actual position sensors used. The M-file is then written to

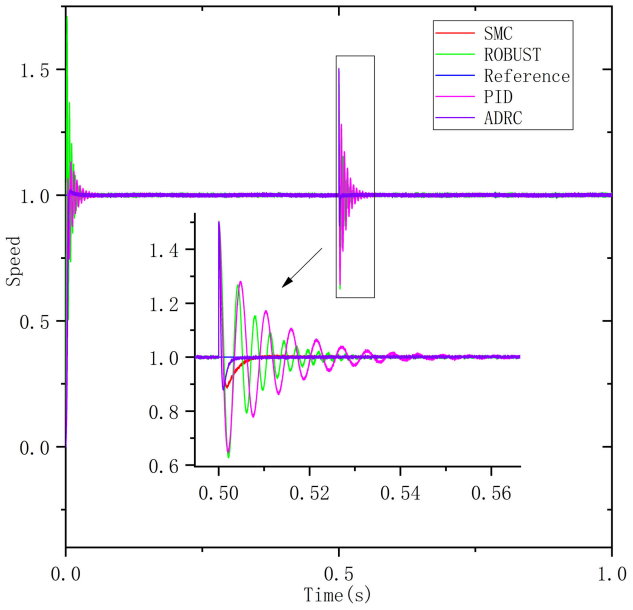

FIGURE 6. The response results of the tracking at $d(t) = 0$ with an impulse perturbation of amplitude 0.5 applied at 0.5 seconds.

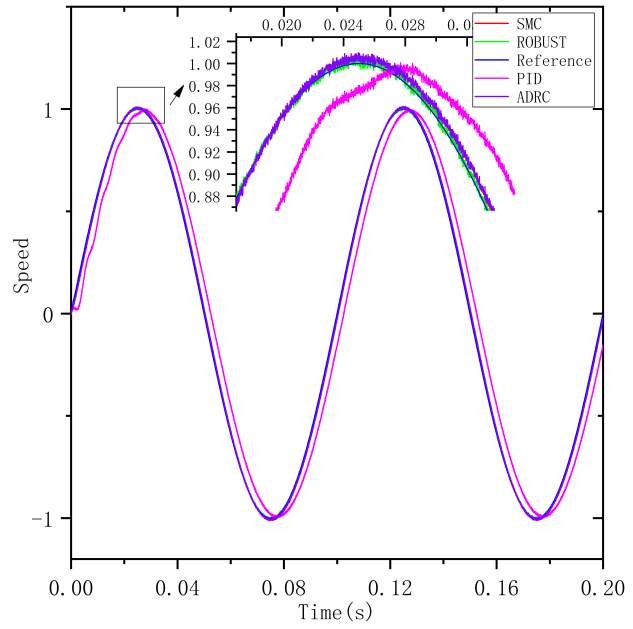

FIGURE 7. The response results of the tracking $\sin(20\pi t)$ with $d(t) = sin(4\pi t)$.

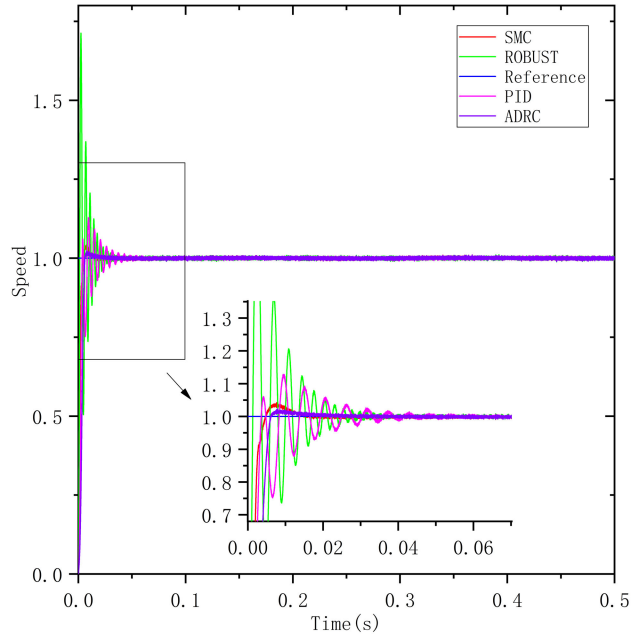

FIGURE 8. The response results of the tracking unit step with $d(t) = sin(4\pi t)$.

TABLE 5. Parameters of the DE algorithm.

Item	Value
population size	90
F_{min}	1e-3
F_{max}	1
CR_{max}	0.9
CR_{min}	0.3
K_1	1
K_2	3

TABLE 6. Optimisation range for position loop ADRC parameters.

Parameter	max	min
r	15	3
h_0	-1	-6
β_1	6	1
β_2	3	1
α_1	0	-4
α_2	0	-4
δ	0	-4
$\hat{b}$	0	-4
$\hat{\beta}_1$	5	2
$\hat{\beta}_2$	5	2
$\hat{\beta}_3$	5	2

implement the external DE algorithm and Simulink is called to complete the algorithm to tune the parameters of controller. The parameters of the DE algorithm are set as shown in Table 5, and the controller search range is shown in Table 6.

The fitness of optimal individuals at each generation during progression is shown in Fig. 10, from which it can be seen that the population clearly stops evolving after the 40th generation. According to the selection of the fitness function, the maximum value of the fitness is clearly 1, while the current fitness is stable at 0.88992007. The main reason is that the adaptation cannot reach 1 even when the control is at its best due to the limitations of the physical characteristics of the system itself.

The purpose of the position loop is to filter out low frequency vibrations from the vehicle using the ADRC algorithm with its good anti-disturbance capability. Thus, when tracking a given signal $sin(0.1 \cdot 2\pi t)$ as shown in Fig. 9, the signal $0.5sin(4\pi t)$ is added to simulate the actual tracking situation. As can be seen from the graphs, the controllers

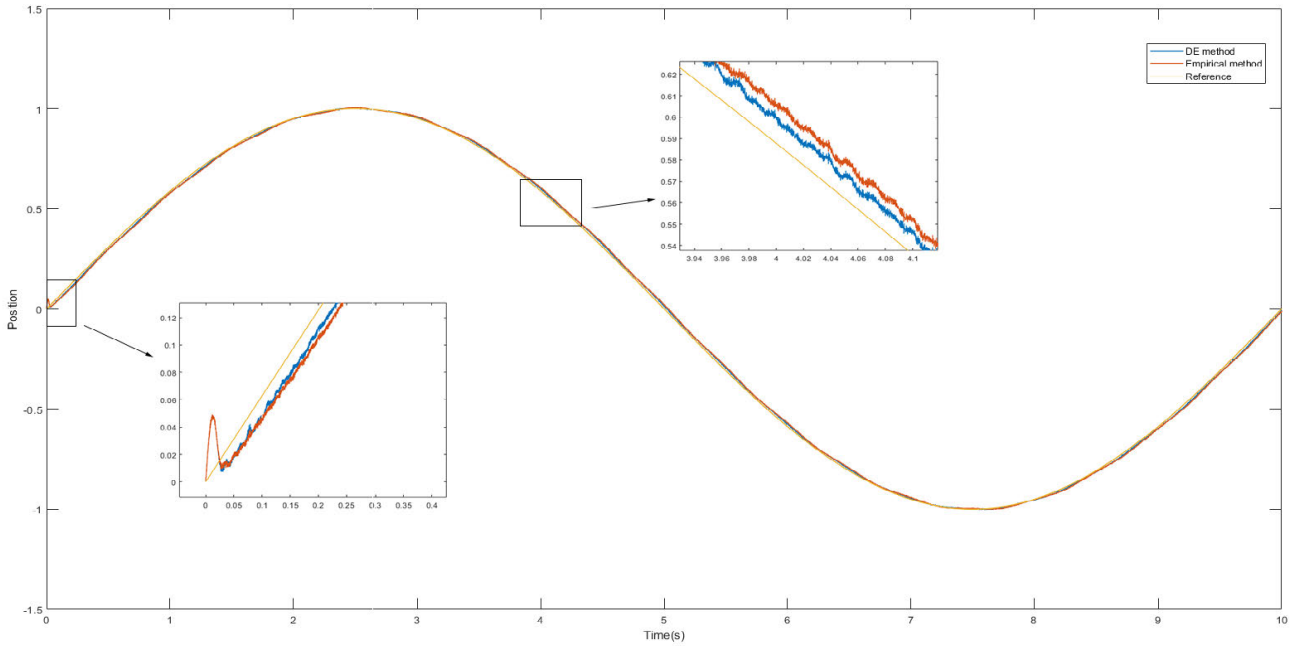

FIGURE 9. Comparing the tracking results of the empirical tuning and DE algorithms.

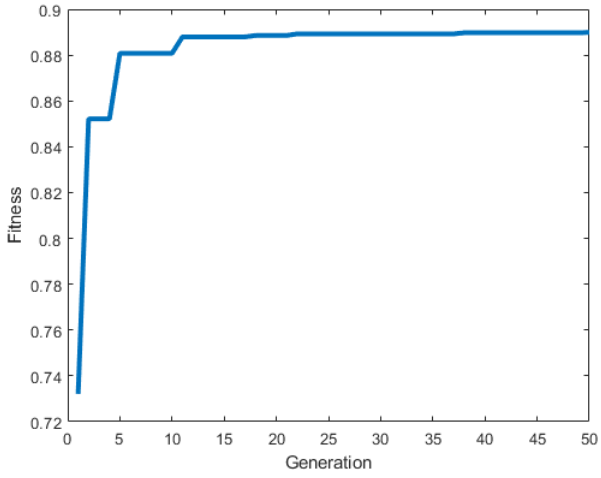

FIGURE 10. Evolutionary optimal individual fitness per generation.

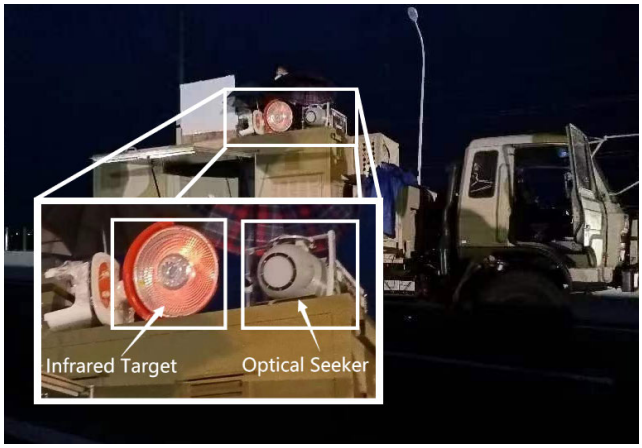

FIGURE 11. Simulated target.

TABLE 7. Parameters of the simulated target and the AIM-9X.

Item	Simulated Target	AIM-9X
waveband	3.7-4.8 μ m	3-5μm
pixel size	30 μm	15/30 μm
Number of pixels	320×256	128×128
Aperture	60mm	about 60mm

TABLE 8. Results of the experiment.

Item	A_RMS(mrad)	E_RMS(mrad)
Experiment A	0.0660	0.0752
Experiment B	0.1938	0.5199
Experiment C	0.2187	0.4277
Experiment D	0.2138	0.5068

are close to each other in terms of control capability under both tuning methods, but the controller with the parameters rectified by the DE algorithm will have a better suppression of disturbances.

V. EXPERIMENTS

To verify the effectiveness of the proposed algorithm, experiments were executed using the equipment shown in Fig. 11 and Fig. 12. Optoelectronic tracking equipment on the carrier vehicle carries out tasks such as target tracking and laser firing. The simulated target consists mainly of a target with infrared characteristics and an optical seeker. A comparison of the performance parameters of the simulated guidance head and the AIM-9X is shown in Table 7. When the equipment is in operation, the infrared characteristics of the simulated target are first captured by the infrared camera and the off-target values are generated and transmitted to the servo

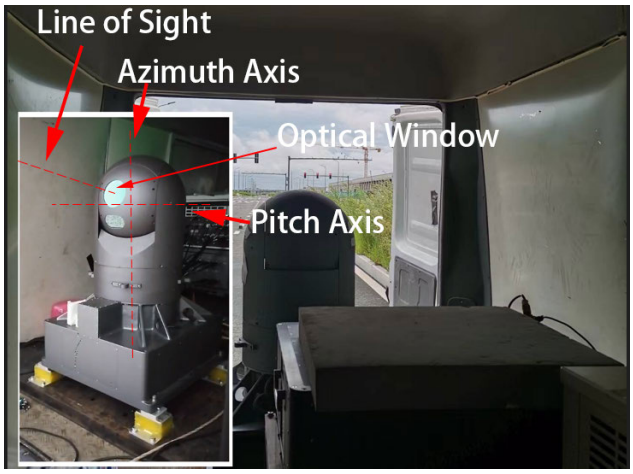

FIGURE 12. Optoelectronic tracking equipment.

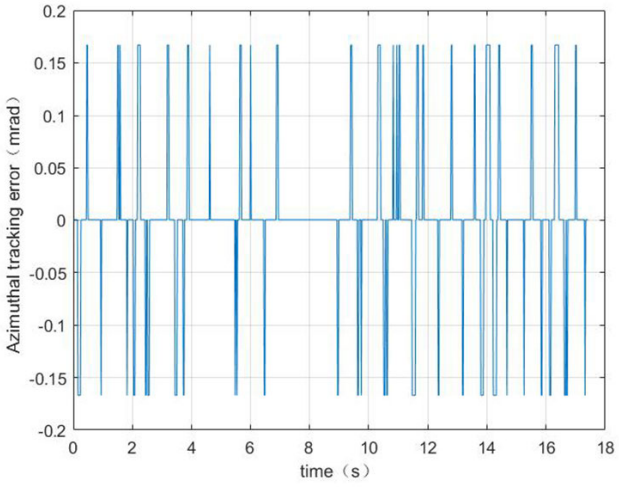

FIGURE 13. Azimuthal tracking error of experiment A.

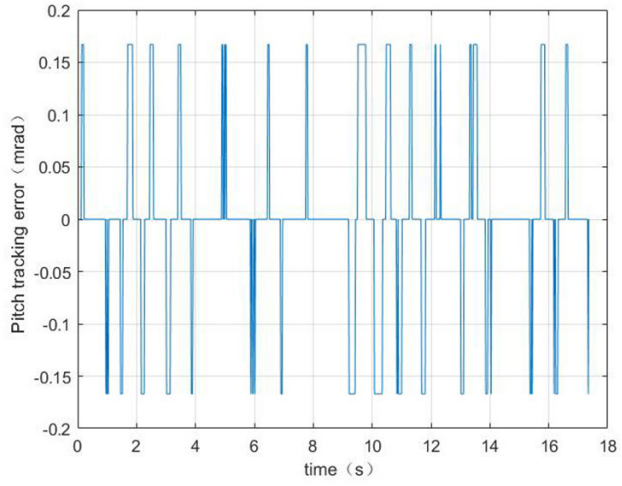

FIGURE 14. Pitch tracking error of experiment A.

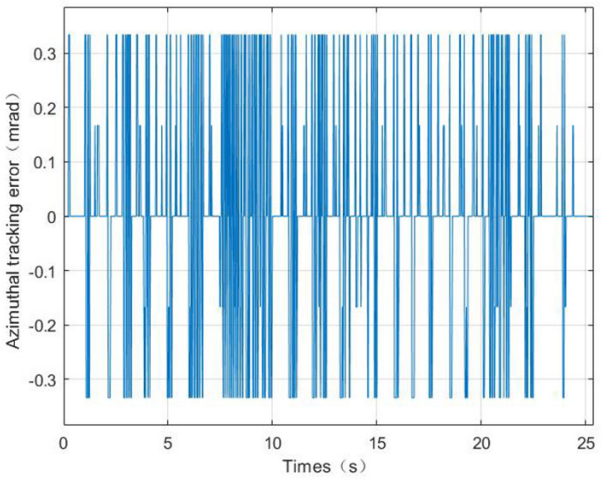

FIGURE 15. Azimuthal tracking error of experiment B.

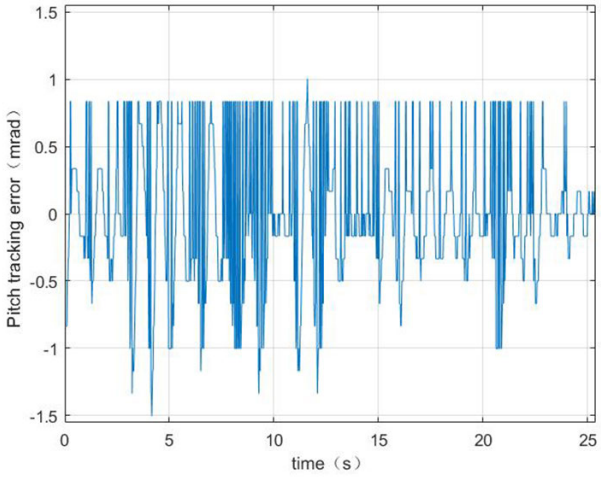

FIGURE 16. Pitch tracking error of experiment B.

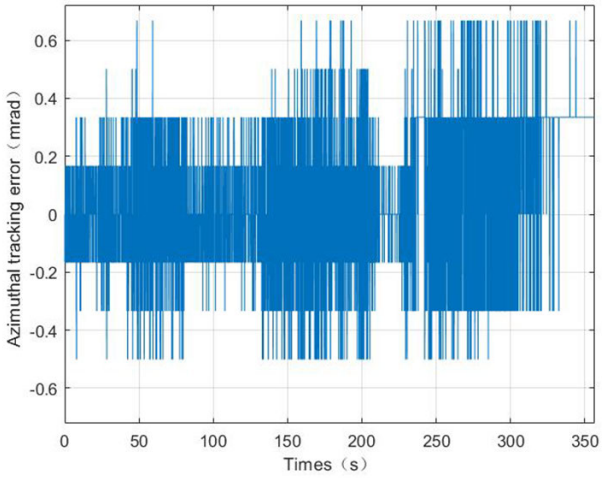

FIGURE 17. Azimuthal tracking error of experiment C.

system. The servo system drives the motor on the azimuth axis and the motor on the pitch axis to turn the corresponding angle according to the value of the off-target quantity, and the line of sight (LOS) of optoelectronic tracking equipment pointing at the target. When the target is locked on by the system, a blinding laser is fired to strike the optical seeker of the simulated target.

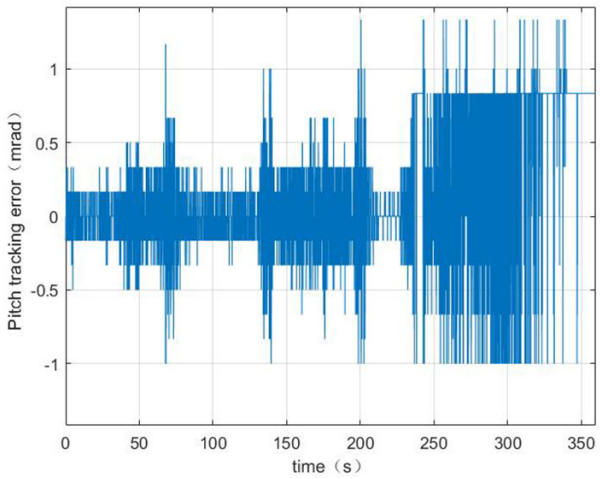

FIGURE 18. Pitch tracking error of experiment C.

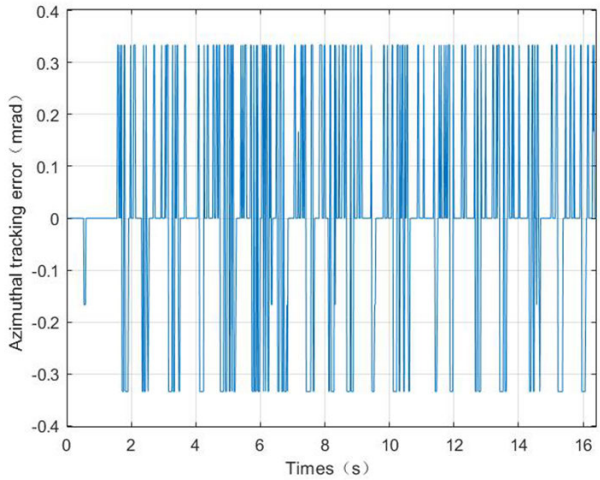

FIGURE 19. Azimuthal tracking error of experiment D.

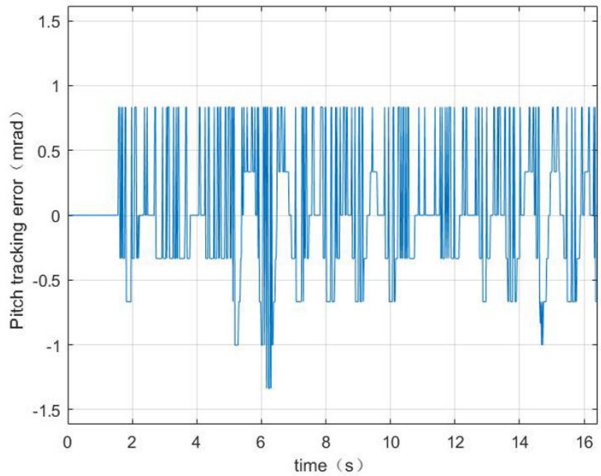

FIGURE 20. Pitch tracking error of experiment D.

A. EXPERIMENT A

The optoelectronic tracking equipment tracks the target from a distance of 1.5Km, with both the target and the equipment remaining stationary. The variation of the off-target during tracking is shown in Fig. 13 and Fig. 14. The tracking results

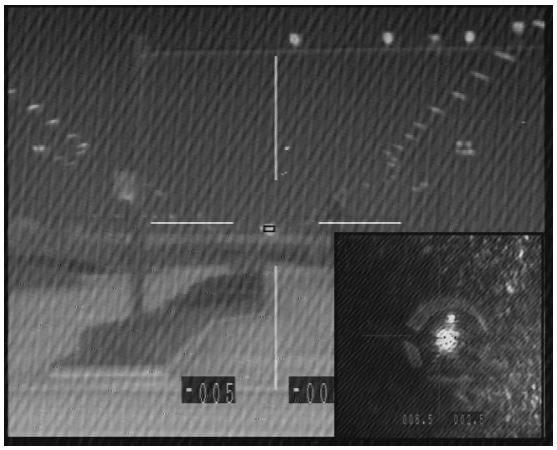

FIGURE 21. Tracking images of equipment.

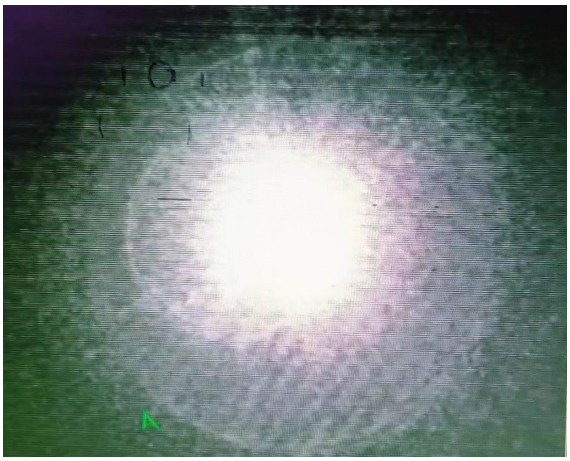

FIGURE 22. Image of optical seeker after laser hit.

for the azimuth (A_{RMS}) and pitch (E_{RMS}) axis are shown in Table 8. The results reveal that the proposed control algorithm is able to achieve a high level of accuracy, with both the target and the device stationary.

B. EXPERIMENT B

The optoelectronic tracking device tracks the target at a distance of 4Km, where both the target and the device are stationary. The device only tracks by virtue of the infrared characteristics of the simulated target. The variation of the tracking error is shown in Fig.15 and Fig. 16. The tracking results for the azimuth and pitch axes are shown in Table 8. Compared to experiment A, there is a large fluctuation in the tracking accuracy of the device at four kilometres. The main reason is the weaker infrared characteristics of the simulated target, which causes several frames over a period of time to fail to capture the target, thus affecting the tracking effectiveness over the whole period of time.

C. EXPERIMENT C

The opto-electronic tracking facility starts at 1.5Km from the target and moves at a speed of 30Km/h to a distance of 3Km from the target. The variation of off-target during vehicle movement is shown in Fig. 17 and Fig. 18. The tracking

results for the azimuth and pitch axes are shown in Table8. During movement, the unevenness of the road surface and the vibration of the vehicle body cause the tracking error to show wide fluctuations. In contrast to experiment A, the pitch axis tracking error varies more dramatically than the azimuth tracking axis error because the disturbance from the road is mostly superimposed on the pitch axis of the device. The road surface is rougher in the latter part of the experiment, resulting in an increase in tracking error in the later moments compared to the earlier ones.

D. EXPERIMENT D

The photoelectric tracking system tracks the target at a distance of 3Km, with both the vehicle and the target at rest. During tracking, the device emits an illuminating laser to actively detect the target optical seeker and emits a blinding laser, the imaging of the target seeker is shown in Fig. 22.The variation of off-target during tracking is shown in Fig. 19 and Fig. 20, and the tracking results for the azimuth and pitch axes are shown in Table 8. The experiments have demonstrated the tracking accuracy of the electro-optical tracking device at 3Km can meet the requirements of the launched laser to accurately hit the missile's optical seeker. Comparing Experiment B and Experiment D, it can be seen that the tracking accuracy at 3Km and 4Km are not very different. This is partly due to the instability of the detector in capturing the target, and partly due to the fact that the water cooler inside the laser is required to work when the main laser is switched on, and the vibrations generated by the water cooler can create a disturbance in the tracking.

VI. CONCLUSION

To improve the tracking accuracy and enhance the robustness of the photoelectric tracking system, this paper proposes a dual closed-loop control method based on ADRC and SMC.And a differential evolutionary algorithm is used to optimise the control algorithm parameters, providing a reference with important implications for parameter tuning. By comparing it with the rest of the commonly used methods, the proposed algorithm shows a high tracking accuracy, a strong tracking capability and a strong robustness. Finally, the effectiveness of the algorithm is strongly proved through experiments, with the system being able to achieve a tracking accuracy of 0.1mrad under the specified tracking conditions.

REFERENCES

[1] Z. Jian and F. Du, "The servo control system of KDUST telescope," *Proc. SPIE*, vol. 9151, Jul. 2014, Art. no. 91513J.
[2] F. Yue, X. Li, C. Chen, and W. Tan, "Adaptive integral backstepping sliding mode control for opto-electronic tracking system based on modified LuGre friction model," *Int. J. Syst. Sci.*, vol. 48, no. 16, pp. 3374–3381, Dec. 2017, doi: 10.1080/00207721.2017.1387315.
[3] Y. Juqing, W. Dayong, and Z. Weihu, "Precision laser tracking servo control system for moving target position measurement," *Optik*, vol. 131, pp. 994–1002, Feb. 2017, doi: 10.1016/j.ijleo.2016.11.214.
[4] J. Q. Han, *Active Disturbance Rejection Control Technique—The Technique for Estimating and Compensating the Uncertainties*. China: Nationl Defense Industry Press, 2008.
[5] Z. Gao, "Scaling and bandwidth-parameterization based controller tuning," in *Proc. Amer. Control Conf.*, Jun. 2003, pp. 4989–4996.
[6] S. Sui and T. Zhao, "Active disturbance rejection control for optoelectronic stabilized platform based on adaptive fuzzy sliding mode control," *ISA Trans.*, vol. 125, pp. 85–98, Jun. 2022, doi: 10.1016/j.isatra.2021.06.020.
[7] M. Cong and T. Zhao, "Active disturbance rejection trajectory tracking control of manipulator based on neural network," in *Proc. Chin. Control Decis. Conf. (CCDC)*, Aug. 2020, pp. 1732–1737.
[8] Z. Zhang, Z. Yang, G. Zhou, S. Liu, D. Zhou, S. Chen, and X. Zhang, "Adaptive fuzzy active-disturbance rejection control-based reconfiguration controller design for aircraft anti-skid braking system," *Actuators*, vol. 10, no. 8, p. 201, Aug. 2021, doi: 10.3390/act10080201.
[9] X. Zhou, H. Gao, B. Zhao, and L. Zhao, "A GA-based parameters tuning method for an ADRC controller of ISP for aerial remote sensing applications," *ISA Trans.*, vol. 81, pp. 318–328, Oct. 2018, doi: 10.1016/j.isatra.2018.08.001.
[10] Z. Yang, C. Lu, X. Sun, J. Ji, and Q. Ding, "Study on active disturbance rejection control of a bearingless induction motor based on an improved particle swarm optimization-genetic algorithm," *IEEE Trans. Transport. Electrific.*, vol. 7, no. 2, pp. 694–705, Jun. 2021, doi: 10.1109/TTE.2020.3031338.
[11] M. Zhang and Q. Li, "A compound scheme based on improved ADRC and nonlinear compensation for electromechanical actuator," *Actuators*, vol. 11, no. 3, p. 93, Mar. 2022, doi: 10.3390/act11030093.
[12] D. Wu, F. Ren, L. Qiao, and W. Zhang, "Active disturbance rejection controller design for dynamically positioned vessels based on adaptive hybrid biogeography-based optimization and differential evolution," *ISA Trans.*, vol. 78, pp. 56–65, Jul. 2018, doi: 10.1016/j.isatra.2017.10.010.
[13] G.-H. Lin, J. Zhang, and Z.-H. Liu, "Hybrid particle swarm optimization with differential evolution for numerical and engineering optimization," *Int. J. Autom. Comput.*, vol. 15, no. 1, pp. 103–114, Feb. 2018, doi: 10.1007/s11633-016-0990-6.
[14] L. Gao, X. Guo, D. Mei, and Z. Qu, "Parameter tuning of active disturbance rejection control based on improved differential evolution algorithm," in *Proc. 7th Int. Conf. Intell. Comput. Signal Process. (ICSP)*, Apr. 2022, pp. 342–346.
[15] X. Yang, Q. Huang, S. Jing, M. Zhang, Z. Zuo, and S. Wang, "Servo system control of satcom on the move based on improved ADRC controller," *Energy Rep.*, vol. 8, pp. 1062–1070, Aug. 2022, doi: 10.1016/j.egyr.2022.02.278.
[16] Y. Z. Zhang, B. S. Jia, Z. Shen, R. Z. Liu, and J. Chen, "Research on SMC-ADRC method of PMSM in mine ventilation system based on ESO," *Eng. Int. Syst.*, vol. 3, pp. 169–177, 2020.
[17] J. Mohorcic and L. Dong, "Extended state observer-based pressure control for pneumatic actuator servo systems," *Control Theory Technol.*, vol. 19, no. 1, pp. 64–79, Mar. 2021, doi: 10.1007/s11768-021-00038-y.
[18] J. Ren, C. Pu, and A. Yu, "Smith control of SCR system based on sliding mode control," *J. Comput. Methods Sci. Eng.*, vol. 21, no. 5, pp. 1293–1304, Nov. 2021, doi: 10.3233/JCM-214933.
[19] G. Chen, Y. Jiang, Y. Tang, and X. Xu, "Revised adaptive active disturbance rejection sliding mode control strategy for vertical stability of active hydro-pneumatic suspension," *ISA Trans.*, vol. 132, pp. 490–507, Jan. 2023, doi: 10.1016/j.isatra.2022.06.008.
[20] Y. Sun, J. Xu, C. Chen, and W. Hu, "Reinforcement learning-based optimal tracking control for levitation system of maglev vehicle with input time delay," *IEEE Trans. Instrum. Meas.*, vol. 71, pp. 1–13, 2022, doi: 10.1109/TIM.2022.3142059.
[21] Z. M. Chen, Z. Y. Wang, and J. G. Zhang, *Sliding Mode Variable Structure Control Theory and Application*. China: Publishing House of Electronics Industry, 2012, p. 8.
[22] Y. Sun, J. Xu, H. Wu, G. Lin, and S. Mumtaz, "Deep learning based semi-supervised control for vertical security of maglev vehicle with guaranteed bounded airgap," *IEEE Trans. Intell. Transp. Syst.*, vol. 22, no. 7, pp. 4431–4442, Jul. 2021, doi: 10.1109/TITS.2020.3045319.
[23] J.-Q. Han and W. Wang, "Nonlinear tracking-differentiator," *J. Syst. Sci. Math. Sci.*, vol. 14, no. 2, pp. 177–183, 1994, doi: 10.12341/jssms09102.
[24] Q. R. Dong, T. Chen, S. J. Gao, Y. K. Liu, J. Q. Zhang, and H. Wu, "Identification of opto-electronic fine tracking systems based on an improved differential evolution algorithm," *Chin. Opt.*, vol. 13, no. 6, pp. 1314–1323, Dec. 2020, doi: 10.37188/CO.2020-0021.
[25] P. Li and G. Zhu, "IMC-based PID control of servo motors with extended state observer," *Mechatronics*, vol. 62, Oct. 2019, Art. no. 102252, doi: 10.1016/j.mechatronics.2019.102252.

[26] G. Flores and M. Rakotondrabe, "Robust nonlinear control for a piezoelectric actuator in a robotic hand using only position measurements," *IEEE Control Syst. Lett.*, vol. 6, pp. 872–877, 2022, doi: 10.1109/LCSYS.2021.3087102.

ZHAOLONG WU was born in Nei Monggol Autonomous Region, China, in 1997. He received the B.E. degree from Shandong University, China, in 2020. He is currently pursuing the joint Ph.D. degree with the University of Chinese Academy of Sciences and the Changchun Institute of Optics, Fine Mechanics and Physics, Chinese Academy of Sciences, China. His research interests include control systems, sliding-mode control, active disturbance rejection control, and digital control based on DSP and FPGA.

ZHAOBING CHEN received the Ph.D. degree from the Changchun Institute of Optics, Fine Mechanics and Physics, Chinese Academy of Sciences, China, in 2011. He is currently a Professor with the Department of Electro-Optical Countermeasure, Changchun Institute of Optics, Fine Mechanics, and Physics, Chinese Academy of Sciences. His research interests include laser countermeasure, airborne laser countermeasure, and opto-mechatronics.

BOHAN XU received the master's degree from Jilin Agricultural University, China, in 2019. He is currently with the Changchun Institute of Optics, Fine Mechanics and Physics, Chinese Academy of Sciences, China. His research interests include optical-mechanical design and assembly.

SHUSHUAI PANG was born in Jilin, China. He received the B.E. degree from Jilin Engineering Normal University, China, in 2019. He is currently with the Changchun Institute of Optics, Fine Mechanics and Physics, Chinese Academy of Sciences, China. His research interests include optical-mechanical design and assembly.

FENG LIN received the master's degree from Jilin University, China, in 2021. He is currently a Research Intern with the Changchun Institute of Optics, Fine Mechanics and Physics. His research interests include research on optical mechatronics, laser echo technology research, image processing, the structure design of precision machinery, and optical systems.